Corrosion Protection Mechanism Study of Nitrite Modified CaAl-LDH in Epoxy Coatings

Junhao Xue , Jingjing Wang * , Yanhui Cao * , Xinyue Zhang , Lill Zhang , Kaifeng Chen , Congshu Huang

Posted Date: 7 June 2023

doi: 10.20944/preprints202306.0495.v1

Keywords: Layered double hydroxide; Epoxy coatings; Corrosion protection mechanism

Article

Corrosion Protection Mechanism Study of Nitrite Modified CaAl-LDH in Epoxy Coatings

Junhao Xue [1,2], Jingjing Wang [1,2,*], Yanhui Cao [1,2,*], Xinyue Zhang [1,2], Lili Zhang [1,2], Kaifeng Chen [1,2] and Congshu Huang [1,2]

[1] Luoyang Ship Material Research Institute, Xiamen 361101, China; ohtlys@sina.cn (X.Z.); xm725ckf@163.com (K.C.)

[2] Science and Technology on Marine Corrosion and Protection Laboratory, Xiamen 361101, China

* Correspondence: jingjing811014@163.com (J.W.); yanhuicao@yeah.net (Y.C.)

Abstract: In this work, nitrite intercalated CaAl-LDH was firstly prepared in this work. Scanning electronic microscopy (SEM) coupled with the energy dispersive spectrometer (EDS) was used to characterize the morphology and element composition of the synthesized powder. Fourier transform infrared spectroscopy (FTIR) was used to characterize the chemical composition and X-ray diffraction (XRD) was used to analyze the structure. The nitrite release curve and the chloride concentration change curve were obtained to study the anion-exchange reaction. The corrosion protection effect of the CaAl-LDH loaded with nitrites towards the carbon steel was evaluated in 0.02 M NaCl solution by electrochemical impedance spectroscopy (EIS). Then the powder was added in the epoxy coating with a percentage of 2% (vs. epoxy resin). The coating morphology and roughness was evaluated by SEM and laser microscopy, and the corrosion protection effect was investigated by EIS in an immersion period of 21 d. Local electrochemical impedance spectra (LEIS) was used to characterize the corrosion development process in micro-corrosion sites. The corrosion product of the scratched area after salt spray exposure was analyzed by EDS and Raman spectroscopy. The corrosion protection mechanism of the CaAl-LDH loaded with nitrites was proposed based on the above experimental results.

Keywords: layered double hydroxide; epoxy coatings; corrosion protection mechanism

1. Introduction

Epoxy coatings have been used as effective coatings to protect metal substrate from serious corrosion. However, some micro-cracks, micropores or defects can be produced during the curing process, which could act as the transportation path of water molecules and aggressive chlorides in the coatings. When the water molecules and aggressive chlorides reach the interface between coating and the underlying substrate, corrosion will be initiated and further propagated if no inhibitors exist in this system [1]. Therefore, to solve this problem, researchers developed lots of methods to prevent corrosion initiation and propagation [2,3].

To enhance the permeation difficulty of water molecules and aggressive chlorides, researchers added 2D materials with high aspect ratio into the polymer matrix, such as graphene, basalt, hexagonal boron-nitride, MXene, layered double hydroxides, etc. [4]. The poor dispersion and serious aggregation limited their application in coatings. Lots effort had been devoted to improve the dispersion state in the epoxy coatings. For example, Yulong Wu et al. grew ZnAl-LDH on the surface of Mxene to inhibit its self-restacking and spontaneous aggregation [5,6]. In addition, Meng Zhang et al. prepared LDH loaded with molybdate on the surface of PDA-modified basalt, which could avoid stacking of LDH platelet and also increased the interfacial compatibility between fillers and epoxy resin [1]. As reported by Seyyed Arash Haddadi et al., the NO_3^- intercalated ZnAl-based layered double hydroxides was used to decorate graphene oxide to prevent the formaton of agglomeration and poor dispersion of graphene oxide [7].

 doi:10.20944/preprints202306.0495.v1

In addition, researchers developed various inhibitor nanocontainers and incorporated them in the epoxy coatings. The nanocontainers mainly include layered double hydroxides (LDHs), mesoporous silica, multiwall carbon nanotubes, polyurea microcapsules, metal-organic frameworks (MOFs), halloysites, montmorillonite, etc. [8–14]. For example, Dashuai Yan et al. used mesoporous silica as the inhibitor container and loaded them with cysteine and iron polyacrylate, which were added into the bottom and top epoxy coating of a double-layered coating system, respectively. The coating exhibited excellent corrosion protection effect [15]. Yanling Jia et al. prepared pH responsive smart nanocontainer via inclusion of inhibitor L-histidine (L-His) in graphene/halloysite nanotubes and applied them as a modifier in waterborne coatings. The driving force of the release of the intercalated inhibitor L-His is mainly resulting from the electrostatic adsorption and the responsive release curve was different in acid and alkaline solutions [16]. I. Mohammadi et al. synthesized cerium loaded Na-montmorillonite (Na-MMT) and incorporated them in the epoxy coating. The active inhibitive performance of the nanoreservoirs can be ascribed to the Ce^{3+} release from the Ce-MMT [17]. Xuteng Xue et al. loaded Na_2MoO_4 and benzotrialoze (BTA) into halloysite nanotubes (HNTs) and obtained Cu-BTA-Na_2MoO_4-HNTs, and this composite demonstrated promising efficient acid-response corrosion protection for the carbon steel [11].

Compared to other micro/nano-containers, the most attractive characteristic of LDHs can be attributed to the anion-exchange capability [18]. This suggested that inhibitors can be released only on demand. When aggressive anions such as chlorides appeared in the external environment, they can be adsorbed into the interlayer space and correspondingly the intercalated inhibitor anions can be released to heal the corrosion site and inhibit corrosion propagation. This controlled release of inhibitors depending on the changes of the environment is able to provide effective corrosion protection in a long term. It should be noted that he anion-exchange reaction was influenced by a wide range of factors including pH, temperature, the size and charge of the intercalated anions and the anions in the environment, and the concentration of the anions in the environment [19]. Thus, the anion-exchange capability and kinetics could be adjusted by changing the above factors.

Yanning Chen et al. prepared a graphene oxide (GO)-doped ternary Mg-Al-La layered double hydroxides (LDHs) (ternary L/G-V coating) loaded with vanadate ($V_2O_7^{4-}$). The effective inhibition effect of this L/G-V coating can be attributed to the release of $V_2O_4^{7-}$ and its precipitation on the anodic area of $Mg_4(V_2O_7)_2$. The La cations and vanadate anions play a synergistic role and thus a double self-healing effect [20]. They further developed MOF decorated graphene oxide/MgAl-LDH on the micro-arc oxide coating on AZ31 magnesium alloy [21]. Tatsiana Shulha et al. intercalated two kinds of typical inhibitor including oxalates and vanadates into MgAl-LDH. The results demonstrated that LDH loaded with vanadates is much more effective for the active protection of magnesium than the LDH loaded with oxalates [22]. Mohammad Tabish et al. prepared CaAl-LDH intercalated with 2-mercaptobenzothiazole (MBT) and added them in epoxy coating with different content, and the obtained coating showed self-healing effect to the carbon steel [23]. In recent publications, LDH was frequently used in combination with other species including MOF, ZIF, GO, MXene to obtain better corrosion protection effect in coatings [6,24,25].

In our previous work, the enhanced corrosion protection effect of the coating with addition of LDH was mainly attributed to the physical barrier effect of the incorporated LDH platelets, while the chloride trapping effect caused by the anion-exchange reaction make little contributions when no effective inhibitors were loaded in the LDH interlayer space [26]. In this work, we further worked on the corrosion mechanism study of LDH in epoxy coatings when effective traditional inhibitor anions were intercalated in the LDH gallery. CaAl-LDH intercalated with nitrites was synthesized firstly in this work and added into the epoxy coating. A wide range of characterization methods were used to characterize the LDH powder and the coating. Finally, the corresponding corrosion mechanism was proposed.

 doi:10.20944/preprints202306.0495.v1

2. Experimental

2.1. Materials and Agents

The chemical agents including $Ca(NO_3)_2{\cdot}4H_2O$, $Al(NO_3)_3{\cdot}9H_2O$, $NaNO_3$, NaOH, $NaNO_2$ and Na_2MoO_4 were purchased from Sinopharm Chemical Reagent Co. Ltd. (Beijing, China). The deionzed water was used for solution preparation. The epoxy resin E-44 and the curing agent 2519 were provided by Shanghai Dekun Industrial Co. Ltd. n-butanol was used as the solvent, which was ordered from Baling Petroleum & Chemical Co. Ltd. (Yueyang, China). The Q235 carbon steel was purchased from y Xiamen Qianfeng Mechanical Co. Ltd. (Xiamen, China). The defoaming agents 530, leveling agent 320 and dispersing agent 110 were provided by Bike Chemial Co. Ltd. (Tongling, China).

2.2. LDH Preparation and Modification

The CaAl-LDH was synthesized by co-precipitation method. A mixed solution of 0.5 M $Ca(NO_3)_2$ and 0.25 M $Al(NO_3)_3$ was added dropwisely into 2 M $NaNO_3$ and 3 M NaOH with high dispersion rate at 65℃. The slurry was then transferred into the hydrothermal stainless reactor and subjected to hydrothermal reaction in oven at 120℃ for 24 h. After washing by deionized water and ethanol, the obtained reactant was finally dried at 60℃ for 48 h and it was labeled as CaAl-LDH.

1g CaAl-LDH was added into 100 mL 0.1 M $NaNO_2$ and the solution was stirred rigorously for 24 h at room temperature in ambient atmosphere. Then the solution was centrifuged at 8000 rpm for 5 min and the obtained solid was subjected to drying in oven for 48 h at 60℃. The obtained sample was labeled as CaAl-LDH-NO_2^-. For the preparation of CaAl-LDH-MoO_4, 0.1 M Na_2MoO_4 was used to replace 0.1 M $NaNO_2$ instead as described above.

2.3. LDH Characterization

The morphology of CaAl-LDH, CaAl-LDH-NO_2^-, CaAl-LDH-MoO_4^{2-} was observed by scanning electronic microscopy (SEM, ZEISS ULTRA55, Carl Zeiss AG Co. Ltd., Dresden, Germany). The elemental composition of these samples was detected by the coupled energy dispersive spectrometer (EDS, Carl Zeiss AG Co. Ltd., Dresden, Germany). Fourier transform infrared spectroscopy (FTIR, Nicolet IS10, Thermo Fisher Scientific Co. Ltd., Waltham, MA, USA) was used to characterize the chemical composition of the synthesized LDH samples, the scanning was from 400 cm-1 to 4000 cm^{-1} and the resolution was 4 cm^{-1}. X-ray diffraction (XRD, X'Pert PRO, Malvern PANalytical Co. Ltd., Almelo, Netherlands) was used to analyze the structure of LDH, and it was scanned from 5 to 80°, and the scanning rate was 10 °/min. The corrosion protection ability of the prepared LDH powders in 0.02 M NaCl solution with a concentration of 5 g/L towards carbon steel was evaluated by Autolab electrochemical workstation. The scanned frequency was from 10^5-10^{-2}Hz and the adopted sinusoidal disturbance was 10 mV. The EIS spectra were recorded every day in an immersion period up to 7 d.

2.4. Coating Preparation

Component A was prepared according to the following procedure. 4g LDH-NO_2^- was added in 100 mL n-butanol. It was subjected to rigorous stirring for 20min and was then ultrasonically dispersing for 30 min. Afterwards, the n-butanol was mixed with 200g epoxy resin (E-44). In addition, 2g defoaming agents 530, 2g leveling agent 320 and 2g dispersing agent 110 were also added into the above mixture. The mixture was subjected to rigorous dispersion with a dispersing rate of 1000 r/min. The curing agent 2519 was used as component B. Please note that component A and B was mixed with a ratio of 300:84 using a wooded stick. This mixture was applied on the carbon steel plate (70mm × 150mm) using a brush. After curing for 24h, the mixture will be applied on the coated carbon steel plate again. The total thickness of the coating was controlled to 120 μm ± 20 μm. For comparison, component A without and with 4g LDH was also prepared.

Preprints (www.preprints.org) | NOT PEER-REVIEWED | Posted: 7 June 2023 doi:10.20944/preprints202306.0495.v1

2.5. Coating Characterization

The top-view and side-view morphology of the prepared epoxy coating was characterized by scanning electronic microscopy (SEM). The 3D morphology and the roughness was measured by laser microscopy (KEYENCE, VK-X150, Japan) with a laser wavelength of 658 nm. The corrosion protection ability of the coating was evaluated by EIS. The EIS was measured by Electrochemical Impedance Analyzer (Wuhan Kesite Instrument Co. Ltd., Wuhan, China). The scanned frequency was from 10^{5}-10^{-2} Hz and the adopted sinusoidal disturbance of 10 mV. The EIS spectra were recorded until 21d. In addition, the corrosion protection effect was also investigated by salt spray test for 7 days according to GB/T 1771-2007. Before the salt spray test, the coating sample was scratched artificially and the underlying bare metal substrate can be exposed to the corrosive salt spray. After the salt spray test, the optical images of the samples were captured. The rust was removed from the scratched area and EDS results of the rust were obtained. In addition, DXR Raman Microscope (ThermoFisher) was also used to characterize the composition of the rust to analyze the difference of different samples with an excitation laser wavelength of 633 nm. The localized electrochemical impedance spectroscopy (LEIS) was used to evaluate the self-healing behavior of the samples. The amplitude was 10mV and the adopted frequency was 50 Hz. The scanning area is 4mm × 4mm. The corresponding spectra was recorded after exposing to 3.5 wt.% NaCl for 1 h, 24 h and 48 h.

3. Results and Discussion

3.1. Characterization of the Synthesized LDH Powders

As can be seen from Figure 1a,b, the synthesized CaAl-LDH presented hexagonal shape with wide distributions of the sizes. The size of most CaAl-LDH platelets was larger than 2 μm approximately. The obvious aggregations of CaAl-LDH also appeared as marked by the red circles in Figure 1b. The EDS results indicated that the CaAl molar ratio was 1.70, which was close to the theoretical value of 2.

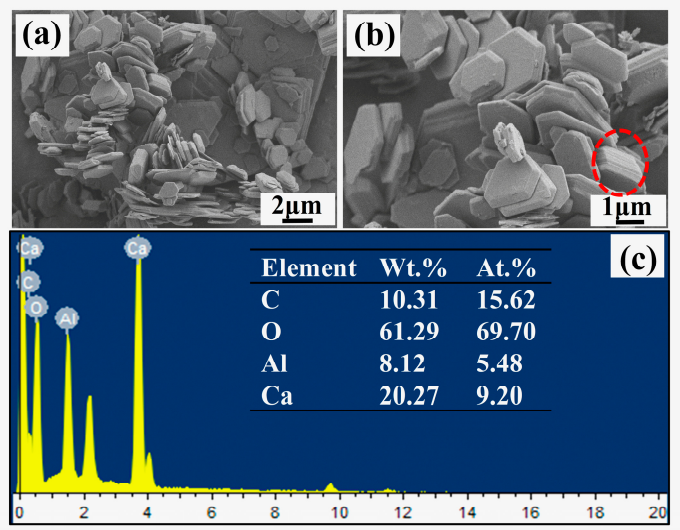

Figure 1. The SEM and EDS results of CaAl-LDH.

The element distribution of CaAl-LDH was shown in Figure 2. It can be seen that the Ca, Al and O distributed uniformly corresponding to the LDH platelets in Figure 2a, while the distribution of C element was different from the other three elements as the detected substrate of the conductive adhesive tape was rich in C element.

Preprints (www.preprints.org) | NOT PEER-REVIEWED | Posted: 7 June 2023 doi:10.20944/preprints202306.0495.v1

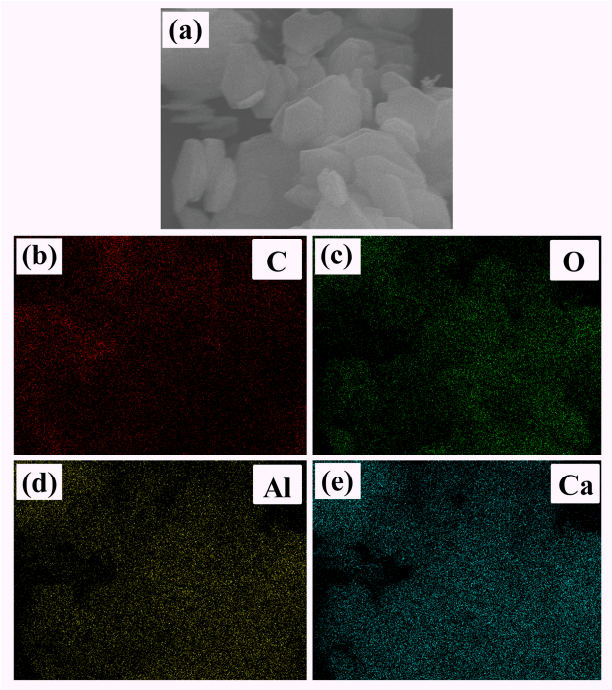

Figure 2. The element distribution of CaAl-LDH.

According to Figure 3a,c, the morphology of CaAl-LDH-NO_2^- was similar to that of pristine CaAl-LDH without obvious changes. However, after modification by Na_2MoO_4, the obtained CaAl-LDH-MoO_4^{2-} presented flower-like morphology, which was completely different from that of CaAl-LDH and CaAl-LDH-NO_2^-. It was probable the CaAl-LDH suffered from significant phase transformation during the immersion process in the Na_2MoO_4 solution. In addition, the EDS results of CaAl-LDH-NO_2^- showed a CaAl mole ratio of 1.87, which was close to the theoretical value of 2. The N element from NO_2^- cannot be detected probably due to the fact that N belonged to light element. Based on the EDS result of CaAl-LDH-MoO_4^{2-} in Figure 3f, a significant amount of Mo element appeared in the EDS spectrum, indicating the existence of MoO_4^{2-}. Al element became negligible, this result suggested that LDH structure may be destroyed and some new substance was formed probably during the modification process. Other characterizations were needed to be performed to further define the formed products.

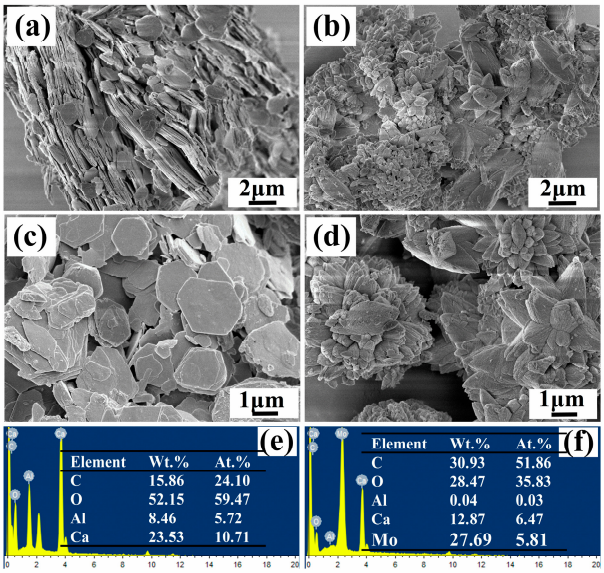

Figure 3. The morphology and element composition of CaAl-LDH-NO_2^- and CaAl-LDH-MoO_4^{2-}.

Preprints (www.preprints.org) | NOT PEER-REVIEWED | Posted: 7 June 2023 doi:10.20944/preprints202306.0495.v1

Figure 4 shows the XRD results of CaAl-LDH, CaAl-LDH-NO_2^- and CaAl-LDH-MoO_4^{2-}. It can be seen from Figure 4a that the CaAl-LDH and CaAl-LDH-NO_2^- present well-defined peaks of LDH corresponding to (003) plane and (006) plane [27], while the sample of CaAl-LDH- MoO_4^{2-} only presented peaks related to $CaMoO_4$ (PDF29-0351) and the peaks related to LDH have disappeared completely. The peak of (003) plane of CaAl-LDH and CaAl-LDH-NO_2^- occurred at 10.2 and 11.1, respectively. The corresponding gallery height was calculated to be 8.67 and 7.96, respectively. According to Figure 4b, some peaks attributed to $CaCO_3$ can be observed in the XRD spectra of CaAl-LDH, indicating the formation of impurities in the LDH synthesis process. The intensity of CaAl-LDH-NO_2^- decreased obviously in comparison with CaAl-LDH, suggesting the declined crystallinity of LDH during the modification process in $NaNO_2$ solution. The peaks related to $CaMoO_4$ can be defined clearly, corresponding to different planes of $CaMoO_4$, which have been marked in Figure 4b. It can be concluded that the CaAl-LDH underwent structure transformation during immersion in the Na_2MoO_4 solution, CaAl-LDH may dissolve and insoluble $CaMoO_4$ was formed finally. This result was in good accordance with the aforementioned SEM and EDS results in Figure 3b,d,f. In the reported literature, Na_2MoO_4 was used to modify LDH such as ZnAl-LDH and MgAl-LDH frequently and the obtained LDH usually presented excellent corrosion inhibiting properties [28–30]. In this work, Na_2MoO_4 was used to modify CaAl-LDH for the first time and it can be found that the main product resulted to be $CaMoO_4$, demonstrating that MoO_4^{2-} inhibitor anions cannot be used for the modification of CaAl-LDH. This newly reported phenomenon was discovered for the first time, which could provide useful instruction information for the researchers and engineers in the relevant field.

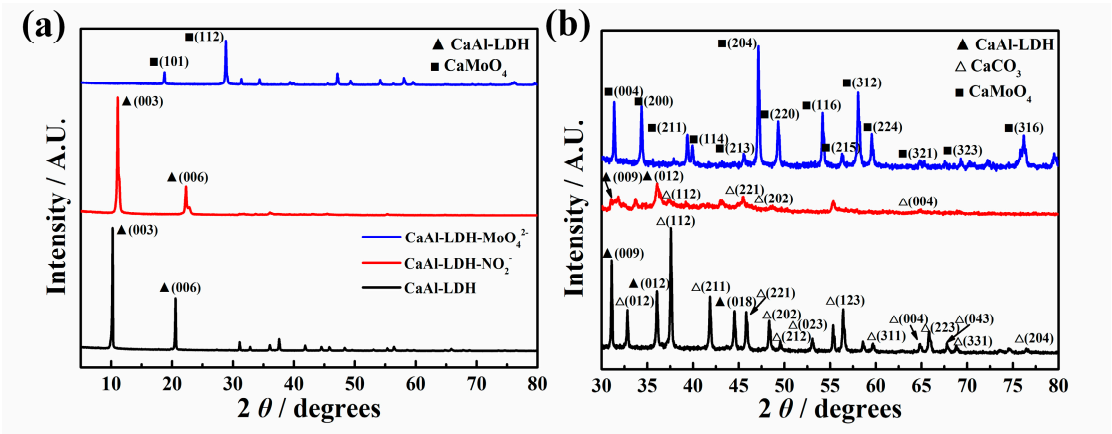

Figure 4. XRD results of different samples (a) from 5-80°; (b) the magnified XRD spectrum from 30 to 80°.

The FTIR results of different samples CaAl-LDH, CaAl-LDH-NO_2^- and CaAl-LDH-MoO_4^{2-} are listed in Figure 5. The peaks around 530 and 420 cm^{-1} in the FTIR spectrum of CaAl-LDH and CaAl-LDH-NO_2^- can be attributed to M-O and M-OH in the LDH lattice, respectively [23]. The peaks around 1635 cm^{-1} in the three curves can be ascribed to bending stretching of H_2O molecules [30]. As for CaAl-LDH, the spectrum in the range of 1290-1420 cm^{-1} was magnified as shown in Figure 5b, the peak at 1352 cm^{-1} belong to the carbonates and the peak at 1384 cm^{-1} can be attributed to nitrites [31]. The peak at 1270 cm^{-1} at the curve of CaAl-LDH-NO_2^- was due to the characteristic stretching of NO_2^- [32]. The broad peak around 791 cm^{-1} in the curve of CaAl-LDH-MoO_4^{2-} was due to Mo-O stretching vibration in MoO_4^{2-} tetrahedrons [28].

Preprints (www.preprints.org) | NOT PEER-REVIEWED | Posted: 7 June 2023 doi:10.20944/preprints202306.0495.v1

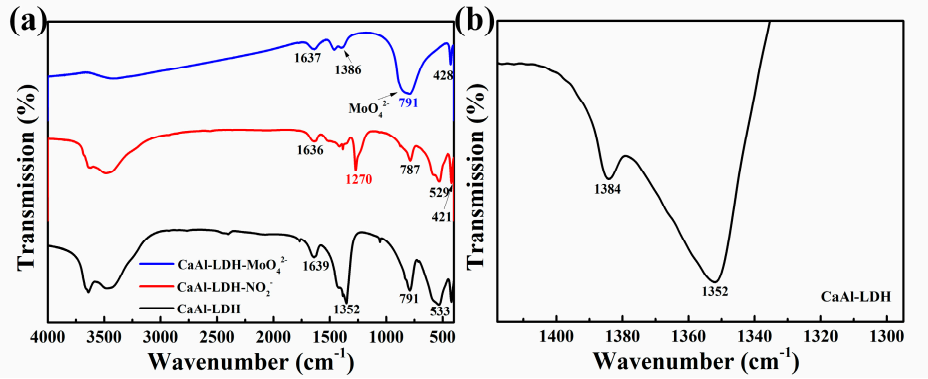

Figure 5. FTIR results of CaAl-LDH, CaAl-LDH-NO_2^- and CaAl-LDH-MoO_4^{2-}.

3.2. Corrosion Protection Ability of the Synthesized LDH Powders in 0.02 M NaCl Solution

In order to evaluate the corrosion protection ability of the synthesized LDH-NO_2^- on the carbon steel, it was added into 0.02 mol/L NaCl with a concentration of 5g/L. For comparison, the EIS measurements of carbon steel in blank NaCl solution and in NaCl solution with 5 g/L LDH were also performed. The EIS results were recorded in an immersion duration of 7 d. Both the Nyquist and Bode plots were presented in Figure 6. According to Figure 6a1–b1 and Figure 6a2–b2, the impedance arc of the sample in blank NaCl solution and in NaCl solution with 5 g/L LDH decreased remarkably after immersion of 1 days in comparison with that of 2 h. The impedance presented a decreasing trend in this immersion period of 7 d in spite of some small fluctuations. According to Figure 6b1–b2, the impedance values at 0.01 Hz of the carbon steel in NaCl solution with 5 g/L LDH were more than one magnitude larger than that of the carbon steel in blank NaCl solution, which may be due to the chloride adsorption effect based on the anion exchange characteristic and the enhanced physical barrier effect caused by the plate-like morphology of LDH. In addition, the phase angle peak in Figure 6c2 was much broader than that in Figure 6c3, indicating certain corrosion protection of LDH powder in NaCl solution towards the carbon steel. When LDH-NO_2^- was added in the 0.02 M NaCl solution (Figure 6a3–b3), the obtained impedance arc became much larger than that in the blank NaCl solution and the NaCl solution with addition of 5g/L LDH. The impedance values at the low frequency of 0.01 Hz was one magnitude larger than that of the carbon steel immersed in NaCl solution with addition of 5g/L LDH, indicating enhanced corrosion protection effect of LDH-NO_2^- compared with that of LDH. Accordingly, the phase angle peak in Figure 6c3 was much broader than that in Figure 6c2. The equivalent circuit containing one time constant in Figure 6d was used to fit the EIS data, where R_s was solution resistance, the R_{ct} was the charger transfer resistance related to the electrochemical corrosion reaction and the Q_{dl} meant the double layer capacitance, which was used here to replace an ideal capacitor due to the non-homogeneity of the carbon steel surface in this system [33]. The Fitting results of the above EIS data were shown in Figure 6e,f. According to Figure 6e, the R_{ct} values of the sample immersed in NaCl solution with 5 g/L LDH-NO_2^- indicated a slightly rising trend with the increased immersed time and at least one magnitude higher than other samples, in contrast, the R_{ct} values of the sample immersed in blank NaCl solution and in NaCl solution decreased continuously. In addition, the C_{dl} values of various samples presented a different trend in comparison with that of R_{ct} values. According to the literature, C_{dl} measures the numbers of the electrochemically active sites in the coating/substrate interface [26,34]. The C_{dl} of the carbon steel in blank NaCl solution presented the largest values and the corresponding value of the carbon steel in NaCl solution with 5 g/L LDH was lower, however, this value was still larger than that of carbon steel in NaCl solution with 5 g/L LDH-NO_2^-. This result indicated that corrosion can be effectively prevented in the presence of LDH-NO_2^- in this system. In Figure S1, after the addition of LDH-MoO_4^{2-}, the corrosion resistance of the carbon steel was a little bit larger than that of the carbon steel in blank solution and much smaller than that of the sample with LDH and LDH-NO_2^-, which can be probably due to the formation of $CaMoO_4$ as verified in the SEM results in Figure 3 and the XRD results in Figure 4. Therefore, this product was not added in the epoxy coating for further corrosion test. However, the above result

Preprints (www.preprints.org) | NOT PEER-REVIEWED | Posted: 7 June 2023 doi:10.20944/preprints202306.0495.v1

could provide instruction significance in the future LDH modification and some specific inhibitor was nor suitable for modification of certain LDH due to the possible reactions.

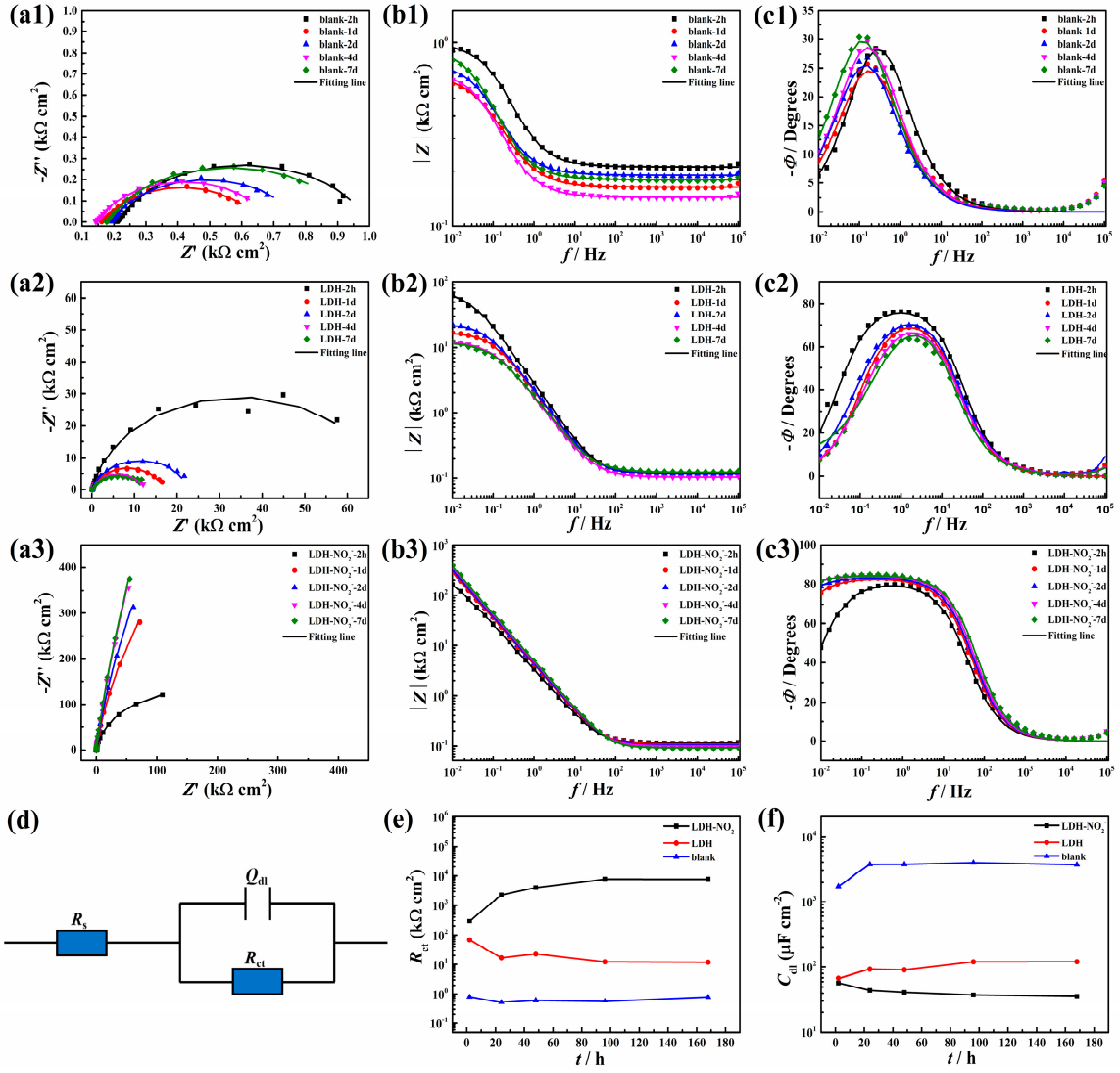

Figure 6. EIS results of the carbon steel after immersed in 0.02 mol/L NaCl without (a1-c1) and with addition of 5g/L LDH (a2-c2) and LDH-NO_2^- (a3-c3); Equivalent circuit used to fit the EIS data (d); The value of R_{ct} changes of different samples along with the immersion time (e); The value of C_{dl} changes of different samples with the immersion time (f).

3.3. The Release Curve of NO_2^- and the Chloride Concentration Decreasing Curve

The anion exchange process between the intercalated NO_2^- in the LDH gallery and the Cl^- in the environment were investigated by obtaining the release curve of NO_2^- from LDH-NO_2^- and the decreasing concentration curve of chloride anions in 0.02 mol/L NaCl solutions with 5g/L LDH-NO_2^- (Figure 7). As shown in Figure 7a, the released NO_2^- accumulated rapidly in the initial period of the first 4 h and the release rate declined gradually with the increased immerse time. After 48 h, the concentration of NO_2^- reached a plateau of higher than 18 mmol/L. However, the anion exchange reaction has not reached a dynamic equilibrium until 48 hours, indicating a controlled release of inhibitor of LDH-NO_2^- in a long term. Correspondingly, the concentration of detected chloride in the solution was decreasing obviously as shown in Figure 7b. Similarly, it can be observed a sharp decrease at the initial immersion period and then the decreasing rate dropped. It can be seen that the chloride concentration did not still reach a steady platform after 48 h. It is clear that the release curve of NO_2^- and the adsorption curve of chloride was in good agreement with each other, and the rapid

Preprints (www.preprints.org) | NOT PEER-REVIEWED | Posted: 7 June 2023 doi:10.20944/preprints202306.0495.v1

anion-exchange reaction in the initial immersion period reflected the burst effect of the anion exchange reaction [19,29]. It is worthy noting that the amount of the released NO_2^- was much larger than that of the absorbed Cl^-. This phenomenon can be probably attributed to the fact that NO_2^- was not only released from the interlayer space though the anion-exchange reaction, the adsorbed NO_2^- on the LDH surface also went into the solution under rigorous stirring.

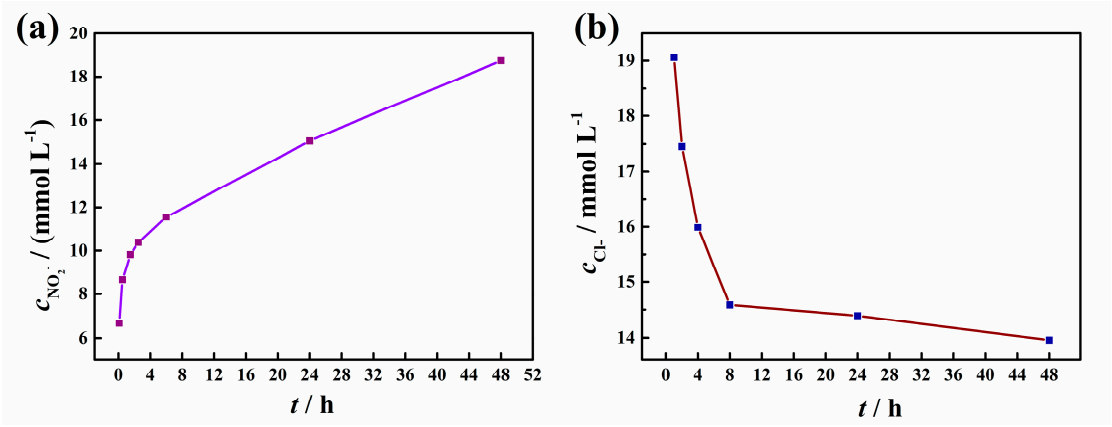

Figure 7. The release curve of NO_2^- from LDH-NO_2^- and the decreasing concentration curve of chloride anions in 0.02 mol/L NaCl solutions with 5g/L LDH-NO_2^-.

3.4. Corrosion Protection Ability of Epoxy Coatings with the Synthesized LDH Powders in 3.5 wt.% NaCl Solution

After applying the epoxy coating on the carbon steel plate, the EIS spectra were measured during long immersion of 14 d. It can be seen that the Nyquist plots of the blank epoxy sample presented two arcs and two phase angle peaks appeared on the Bode plots accordingly. This result indicated that serious corrosion has happened during immersion in 3.5 wt.% NaCl solution. The equivalent circuit with two time constants was used to simulate the EIS data. One time constant was related to the epoxy coatings and the other one corresponded to the electrochemical charge transfer reaction. As for the epoxy coating with addition of 2% LDH, the shape of the EIS spectra changed obviously. It can be seen that the only one arc appeared in the Nyquist diagram and only one wide phase angle peak can be observed on the Bode diagram. The other time constant did not appear, which can be probably due to the fact that corrosion did not occur due to the protection effect of the incorporated LDH. The equivalent with one time constant was used to fit the EIS data and this time constant can be ascribed to the epoxy coatings. According to the figures in Figure 8g–i, one time constant can also be observed and corrosion did not occur in this system. As a result, the equivalent circuit in Figure 8k can be used to simulate the EIS data. Based on the fitted data, the changes of R_c values of different system along with the immersion time were listed in Figure 8l. It can be seen that the R_c value of epoxy sample with LDH was one order of magnitude higher than the blank sample, while the R_c value of epoxy sample with LDH-NO_2^- was two orders of magnitude higher than the sample with LDH further, suggesting the effective corrosion protection of LDH-NO_2^-. In addition to the physical barrier effect of the incorporated LDH plates caused by the increased tortuosity, the presence of the nitrites in this system was able to prevent corrosion initiation and propagation effectively.

Preprints (www.preprints.org) | NOT PEER-REVIEWED | Posted: 7 June 2023 doi:10.20944/preprints202306.0495.v1

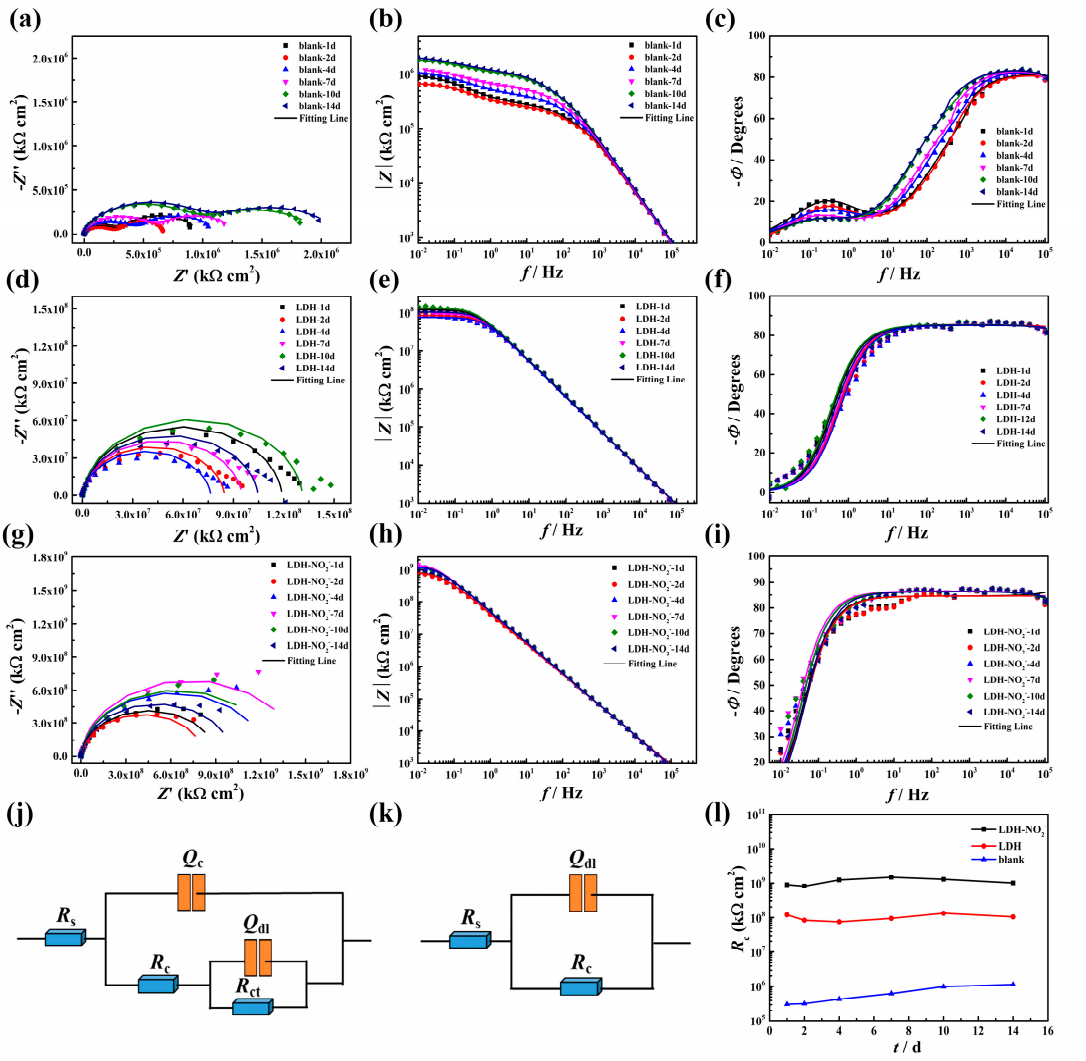

Figure 8. The Nyquist and Bode plots of blank epoxy coatings (a-c); epoxy coatings with addition of 2% LDH (d-f); epoxy coatings with addition of 2% LDH-NO_2^-; (g); Equivalent circuits used to fit EIS data of blank epoxy coatings; (i) Equivalent circuits used to fit EIS data of epoxy coatings with 2% LDH and 2% LDH-NO_2^-; (l) R_c changes along with immersed time.

3.5. Coating Morphology Characterization

The top-view and side-view of the epoxy coating without and with addition of LDH and LDH-NO_2^- are shown in Figure 9. According to the top-view morphology in Figure 9a1–c1, almost no obvious aggregates can be found in the blank epoxy coating (Figure 9a1) and the epoxy coating with 2% LDH-NO_2^- (Figure 9c1), while some aggregates could be found on the surface of epoxy coating with 2% LDH (Figure 9c2). This result demonstrated that the modification of NO_2^- probably enhanced the compatibility of LDH with the coating to some extent. The side-view morphology in Figure 9a2–c2 showed richer information. It can be seen from Figure 9a2 that the some holes appeared in the blank epoxy coating, while the addition of LDH filled the holes to some extent and the compactness of the coating was improved. The addition of LDH-NO_2^- further enhanced the compactness of the coating and no holes or aggregates can be observed in the side-view morphology.

Preprints (www.preprints.org) | NOT PEER-REVIEWED | Posted: 7 June 2023 doi:10.20944/preprints202306.0495.v1

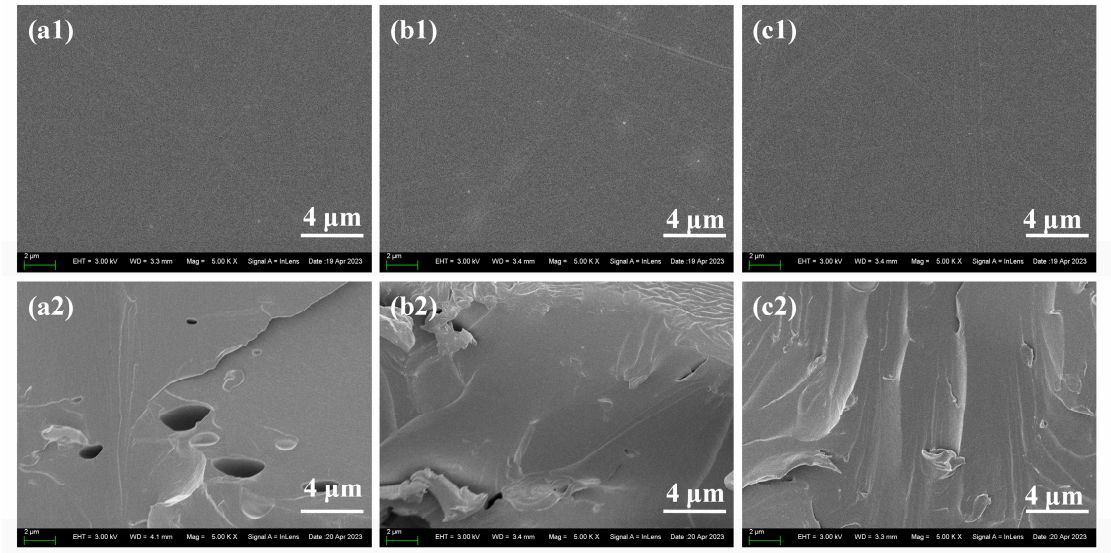

Figure 9. The top-view (a1-c1) and side-view (a2-c2) morphology of blank epoxy coating (a1-a2); epoxy coating with 2% LDH (b1-b2); epoxy coating with 2% LDH-NO2- (c1-c2).

The 3D morphology and roughness of the coating surface were characterized by laser microscopy. It can be seen that the surface of the epoxy coating with 2% LDH was rougher than that of the blank epoxy coating and the coating with 2% LDH-NO_2^-. The changes of the scale bar were in good accordance with the surface morphology and a larger scale bar usually corresponded to a rougher surface. According to the obtained roughness results, the R_a value of the blank epoxy coating, the epoxy coating with 2% LDH and the epoxy coating with 2% LDH-NO_2^- was measured to be 0.309 ± 0.02μm, 0.409 ± 0.08μm and 0.316 ± 0.02μm, respectively. This result was in good agreement with the SEM morphology result in Figure 9. It indicated that the addition of LDH has a negative influence on the compactness of the epoxy coating and the modification of LDH using NO_2^- could improve its compatibility with the epoxy coating, however, the related reasons remain to be further investigated.

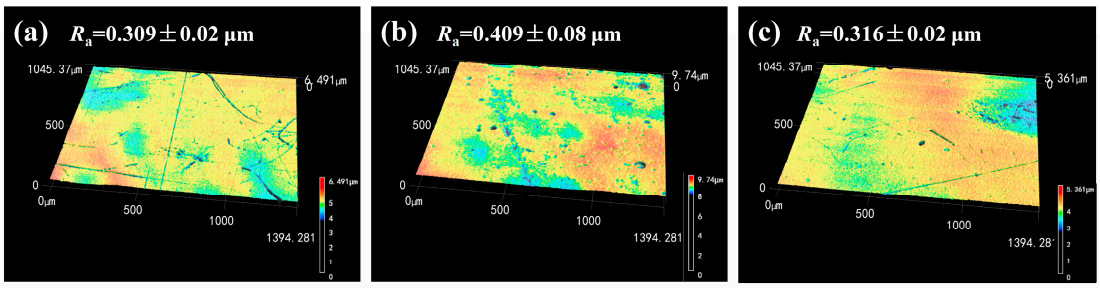

Figure 10. The 3D morphology and roughness of (a) Blank epoxy coating; (b) Epoxy coating with 2% LDH; (c) Epoxy coating with 2% LDH- NO_2^-.

3.6. The Morphology and Corrosion Product Characterization of the Scratched Coating Samples after Salt Spray Test

In order to further study the corrosion protection ability of the added LDH- NO_2^-, the coated samples were scratched artificially and subjected to salt spray test for 7 days. The rust was removed and the optical images were captured, which were shown in Figure 11a1–c1,a2–c2. It can be seen that the corrosion was quite serious on the scratched area of the blank epoxy coating. For the coating with 2% LDH, corrosion was less severe probably due to chloride trapping effect based on the anion-exchange reaction between the intercalated anions and the chlorides and also physical barrier effect as evidenced in Figure 9b2. For the coating with 2% LDH-NO_2^-, corrosion was further inhibited due to the effective inhibiting effect of the released NO_2^- and the enhanced physical barrier effect.

Preprints (www.preprints.org) | NOT PEER-REVIEWED | Posted: 7 June 2023 doi:10.20944/preprints202306.0495.v1

According to the EDS results in Figure 11, the content of Fe element in the scratched area of the epoxy coating with 2% LDH increased compared to the blank epoxy coating, where the atomic percentage of Fe increased from 26.6% to 41.36%. It is worthy noting that this value further increased to 47.77% in the case of the epoxy coating with 2% LDH- NO_2^-.

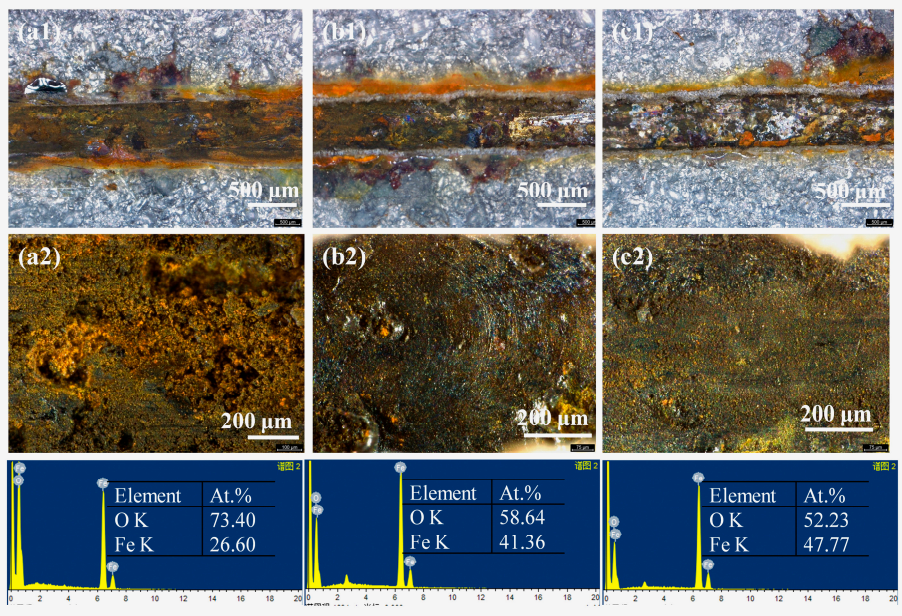

Figure 11. The optical images and the corresponding EDS results of the scratched area of the coating sample after salt spray test for 7 days (a1-a2) blank epoxy coatings; (b1-b2) epoxy coatings with 2% LDH; (c1-c2) epoxy coatings with 2% LDH- NO_2^-.

In order to further analyze the composition of the rust of different scratched sample, Raman spectra were recorded, which were shown in Figure 12. For the blank epoxy coating, the peak around 400 cm-1 and 1300 cm^{-1} corresponded to a-FeOOH and r-FeOOH, respectively. The peak at 285 cm^{-1} was attributed to Fe_2O_3. As for the epoxy coating with addition of 2% LDH and LDH-NO_2^-, the peak around 400 cm^{-1} disappeared completely, and the peak at 1300 cm-1 decreased notably, while the peak around 650-680 cm^{-1} appeared obviously, which can be ascribed to Fe_3O_4. The intensity of this peak further increased for the epoxy coating with 2% LDH-NO_2^- in comparison with that with 2% LDH, while the peak corresponding to r-FeOOH further weakened. The changes of the main corrosion product from a-FeOOH and r-FeOOH to Fe_3O_4 demonstrated that the existence of LDH and LDH-NO_2^- was able to improve the corrosion protection ability of the coating. The LDH-NO_2^- was able to provide more effective protection due to the superior inhibiting effect of NO_2^-.

Preprints (www.preprints.org) | NOT PEER-REVIEWED | Posted: 7 June 2023 doi:10.20944/preprints202306.0495.v1

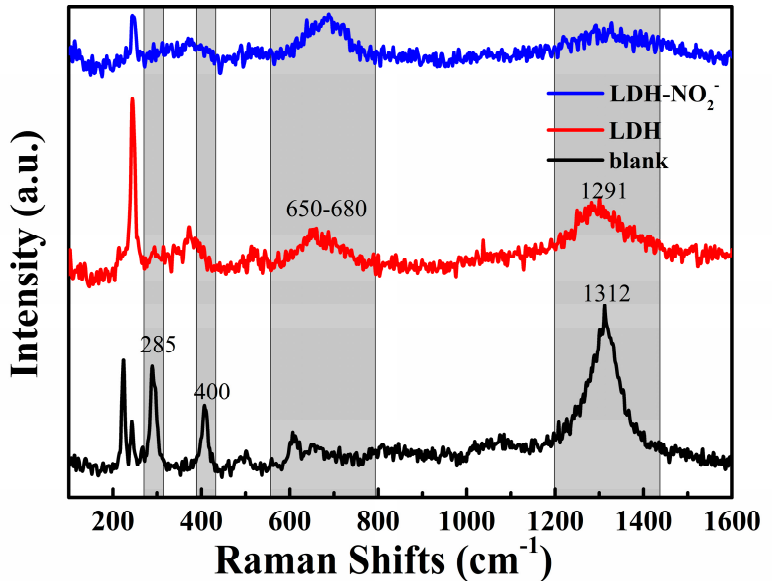

Figure 12. Raman spectra of the rust obtained from the sample in Figure 11.

3.7. Self-Healing Performance of the Coatings

In order to investigate the corrosion protection mechanism of the synthesized LDH, an artificial hole was made by a sharp metal tip on the coating surface. The spectra at 1h, 24h and 48 h were recorded and shown in Figure 13. It can be seen clearly that all the coatings demonstrated a low corrosion resistance in the hole and a higher corrosion resistance in the surrounding area. It is worthy to note that obvious difference can be detected between various coatings. For the blank epoxy coating, serious corrosion occurred at the initial period of 1h and no remarkable changes can be found until the immersion of 48 h. When LDH was included in the epoxy coating, severe corrosion also occurred in this system due to the contact between the exposed metal substrate at the artificial hole and the aggressive NaCl solution, while corrosion was less serious than that of the blank epoxy coating, probably due to the chloride adsorption effect of LDH. As for the coating with LDH-NO_2^-, almost no corrosion can be found at the immersion of 1 h, this attractive phenomenon can be ascribed to the healing effect of the release nitrites from LDH-NO_2^-. Passive film was formed on the metal substrate surface as nitrites could act a strong oxidizer and the corrosion site was healed. However, after immersion for 4 h, corrosion happened again in this healed area probably due to the fact that the passive film was not dense enough and it was broken at the strong attack of chlorides. Corrosion further propagated after immersion for 48h. This result inspired us that the content of LDH-NO_2^- should be further optimized to obtain a more effective protection film at the corrosion area or other more effective corrosion inhibitor could be loaded in LDH to achieve such purpose in the future work.

Preprints (www.preprints.org) | NOT PEER-REVIEWED | Posted: 7 June 2023 doi:10.20944/preprints202306.0495.v1

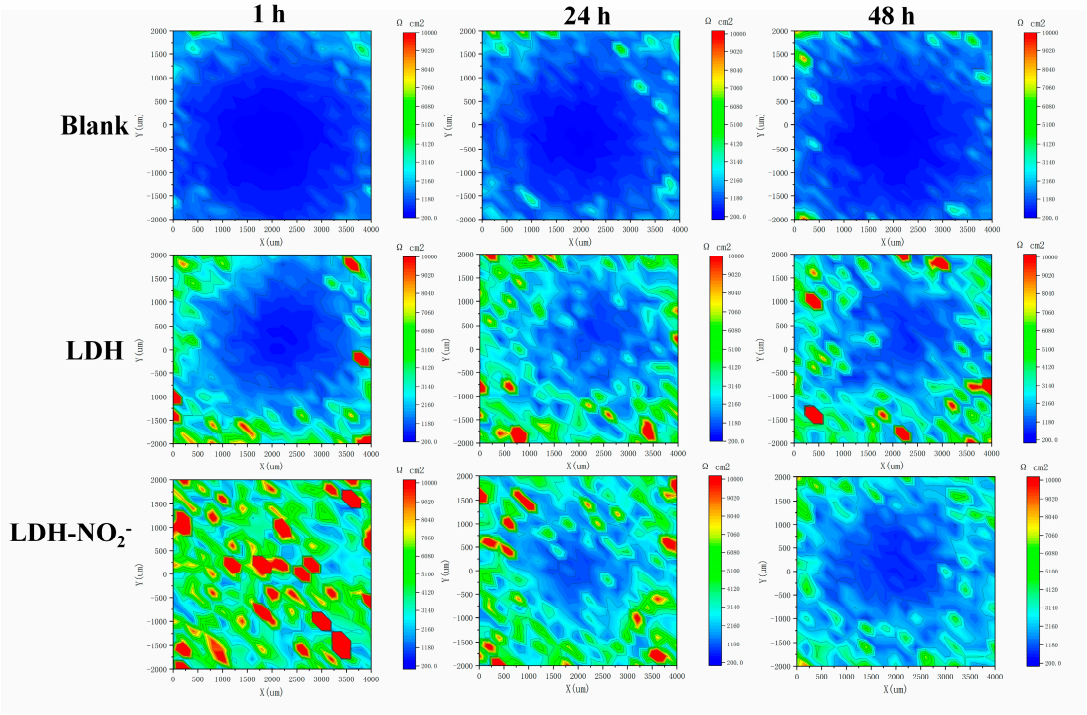

Figure 13. The LEIS maps of blank epoxy coatings, epoxy coatings with 2% LDH, epoxy coatings with 2% LDH-NO_2^- during an immersion period of 1 h, 24 h an 48 h in 3.5% NaCl.

3.8. Corrosion Protection Mechanism

The corrosion protection mechanism of LDH-NO_2^- is shown in Figure 14. As presented in this figure, water molecules and chlorides can be regarded as two main factors resulting in the initiation of corrosion. The enhanced corrosion protection ability of the epoxy coating with addition of LDH-NO_2^- can be attributed to the following two points. On one hand, the existence of LDH platelets was able to improve the tortuosity of the transportation path of water molecules and chlorides, therefore, the time when the aggressive ions and water molecules reach the underlying substrate will be delayed to some extent. On the other hand, the anion-exchange reaction occurred between the intercalated nitrites in the LDH gallery and the aggressive chlorides in the external environment. As a result, the chlorides were adsorbed and the inhibitor nitrites were released. The chloride concentration was finally decreased and the attack towards the substrate will be mitigated. Furthermore, the released nitrites act as inhibitors and heal the corrosion sites, and corrosion propagation can be prevented in this way. Based on the EIS results in Figure 8, it can be concluded that the anion exchange reaction is able to play a significant role in the overall enhanced corrosion protection effect in addition to the physical barrier effect of LDH platelets, which differs from the case where no inhibitors are intercalated. The inhibitor type and loading content can be further optimized to obtain better corrosion protection effect.

 doi:10.20944/preprints202306.0495.v1

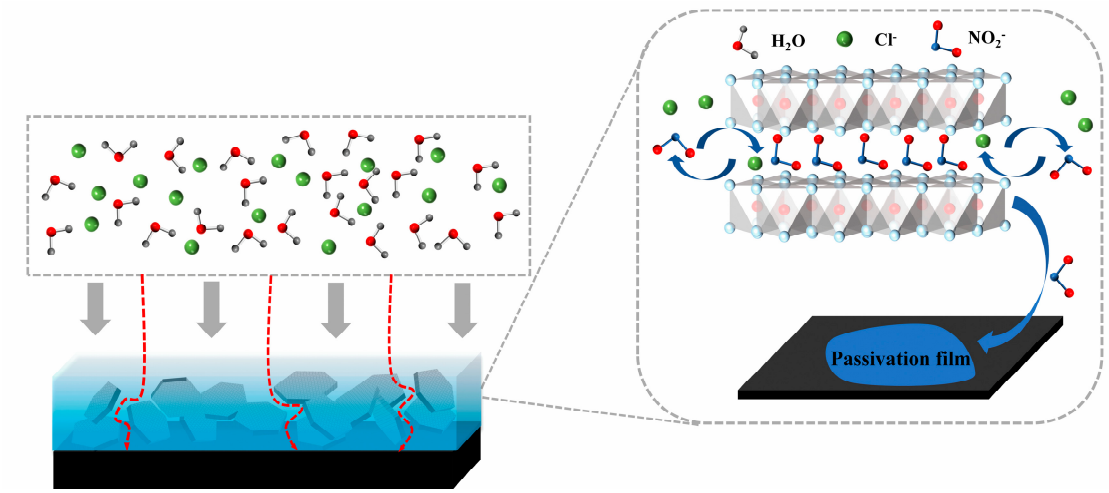

Figure 14. Schematic presentation of the corrosion protection mechanism of LDH- NO_2^-

4. Conclusions

In this work, CaAl-LDH intercalated with nitrites was synthesized and the SEM result indicated plate-like morphology and the XRD result verified the successful intercalation of nitrites in the LDH gallery. The corrosion protection ability of this powder in epoxy coating was evaluated by EIS, and the results demonstrated 2% (vs. epoxy resin) addition in the epoxy coating was able to enable the coating to present enhanced corrosion protection effect with one order of magnitude higher than the coating with 2% CaAl-LDH without no inhibitors. The corrosion protection effect was ascribed to the nitrite release and the chloride trapping based on the anion exchange micro-reaction and the improved physical barrier effect in the coating.

Acknowledgments: This work was funded by Xiamen Natural Science Foundation Project (3502Z20227160) and State Key Laboratory for Marine Corrosion and Protection Foundation (JS220902).

References

1. Zhang, M., et al., *A smart anti-corrosion coating based on triple functional fillers.* Chemical Engineering Journal, 2022. **446**: p. 137078.
2. Zhang, F., et al., Self-healing mechanisms in smart protective coatings: A review. Corrosion Science, 2018. **144**: p. 74-88.
3. Zheludkevich, M.L., J. Tedim, and M.G.S. Ferreira, "Smart" coatings for active corrosion protection based on multi-functional micro and nanocontainers. Electrochimica Acta, 2012. **82**: p. 314-323.
4. Cui, M., et al., Anticorrosive performance of waterborne epoxy coatings containing water-dispersible hexagonal boron nitride (h-BN) nanosheets. Applied Surface Science, 2017. **397**: p. 77-86.
5. Wu, Y., et al., ZnAl-LDH@MXene modified by inhibitor as a nanofiller applied on Mg alloys coating protection. Carbon, 2023. **204**: p. 36-49.
6. Li, C., et al., Cataphoretic deposition of an epoxy coating with the incorporation of Ti3C2Tx@Mg-Al layered double hydroxide for long-term active corrosion protection effect. Progress in Organic Coatings, 2023. **175**: p. 107333.
7. Haddadi, S.A., et al., Sodium lignosulfonate-loaded ZnAl-layered double hydroxide decorated graphene oxide nanolayers; toward fabrication of sustainable nanocomposite for smart corrosion prevention. Journal of Cleaner Production, 2022. **374**: p. 133980.
8. Ren, L., et al., Facile preparation of wear-resistant and anti-corrosion films on magnesium alloy. Surface Engineering, 2022. **38**(1): p. 22-29.
9. Maia, F., et al., Corrosion protection of AA2024 by sol–gel coatings modified with MBT-loaded polyurea microcapsules. Chemical Engineering Journal, 2016. **283**: p. 1108-1117.
10. Xing, X., et al., *Synthesis and inhibition behavior of acid stimuli-responsive Ca-Na2MoO4-HNTs nanocomposite.* Colloids and Surfaces A: Physicochemical and Engineering Aspects, 2018. **553**: p. 305-311.
11. Xing, X., et al., *A novel acid-responsive HNTs-based corrosion inhibitor for protection of carbon steel.* Colloids and Surfaces A: Physicochemical and Engineering Aspects, 2018. **553**: p. 295-304.

12. Karami, Z., et al., Epoxy/layered double hydroxide (LDH) nanocomposites: Synthesis, characterization, and excellent cure feature of nitrate anion intercalated Zn-Al LDH. Progress in Organic Coatings, 2019. **136**: p. 105218-105224.
13. Kopeć, M., et al., Self-healing epoxy coatings loaded with inhibitor-containing polyelectrolyte nanocapsules. Progress in Organic Coatings, 2015. **84**: p. 97-106.
14. Ouyang, Y., et al., A self-healing coating based on facile pH-responsive nanocontainers for corrosion protection of magnesium alloy. Journal of Magnesium and Alloys, 2020.
15. Yan, D., et al., A double-layered self-healing coating system based on the synergistic strategy of cysteine and iron polyacrylate for corrosion protection. Chemical Engineering Journal, 2023. **451**: p. 138995.
16. Jia, Y., et al., Preparation of pH responsive smart nanocontainer via inclusion of inhibitor in graphene/halloysite nanotubes and its application in intelligent anticorrosion protection. Applied Surface Science, 2020. **504**: p. 144496.
17. Mohammadi, I., et al., Enhanced epoxy coating based on cerium loaded Na-montmorillonite as active anti-corrosive nanoreservoirs for corrosion protection of mild steel: Synthesis, characterization, and electrochemical behavior. Progress in Organic Coatings, 2019. **131**: p. 119-130.
18. Guo, X., et al., Layered double hydroxide films: synthesis, properties and applications. Chemical Communications, 2010. **46**(29): p. 5197-210.
19. Cao, Y., et al., Layered double hydroxide (LDH) for multi-functionalized corrosion protection of metals: A review. Journal of Materials Science & Technology, 2022. **102**: p. 232-263.
20. Chen, Y., et al., Synergistic effect of graphene oxide/ ternary Mg-Al-La layered double hydroxide for dual self-healing corrosion protection of micro-arc oxide coating of magnesium alloy. Colloids and Surfaces A: Physicochemical and Engineering Aspects, 2022. **655**: p. 130339.
21. Chen, Y., et al., Development of metal-organic framework (MOF) decorated graphene oxide/MgAl-layered double hydroxide coating via microstructural optimization for anti-corrosion micro-arc oxidation coatings of magnesium alloy. Journal of Materials Science & Technology, 2022. **130**: p. 12-26.
22. Shulha, T., et al., Corrosion Inhibitors Intercalated into Layered Double Hydroxides Prepared In Situ on AZ91 Magnesium Alloys: Structure and Protection Ability. ACS Appl Mater Interfaces, 2023. **15**(4): p. 6098-6112.
23. Tabish, M., et al., Improving the corrosion protection ability of epoxy coating using CaAl LDH intercalated with 2-mercaptobenzothiazole as a pigment on steel substrate. Progress in Organic Coatings, 2022. **165**: p. 106765.
24. Wu, L., et al., Corrosion Resistance of the GO/ZIF-8 Hybrid Loading Benzotriazole as a Multifunctional Composite Filler-Modified MgAlY Layered Double Hydroxide Coating. Langmuir, 2022. **38**(33): p. 10338-10350.
25. Sanaei, Z., A. Shamsipur, and B. Ramezanzadeh, Trisodium phosphate-loaded hierarchically ordered meso-nanoporous ZIF-67/ZIF-8 metal-organic frameworks assembled rGO-Zn-Al-LDH: A multi-level pH-triggered nano-vehicle for epoxy coating long-lasting self-repairing/barrier properties improvement. Chemical Engineering Journal, 2023. **451**: p. 138872.
26. Cao, Y., et al., A Comparative Study of Chloride Adsorption Ability and Corrosion Protection Effect in Epoxy Coatings of Various Layered Double Hydroxides. Coatings, 2022. **12**(11): p. 1631.
27. Zheludkevich, M.L., et al., Active protection coatings with layered double hydroxide nanocontainers of corrosion inhibitor. Corrosion Science, 2010. **52**(2): p. 602-611.
28. Zhang, Y., et al., Fabrication of inhibitor anion-intercalated layered double hydroxide host films on aluminum alloy 2024 and their anticorrosion properties. Journal of Coatings Technology and Research, 2015. **12**(2): p. 293-302.
29. Shkirskiy, V., et al., Factors Affecting MoO42–Inhibitor Release from Zn2Al Based Layered Double Hydroxide and Their Implication in Protecting Hot Dip Galvanized Steel by Means of Organic Coatings. ACS Applied Materials & Interfaces, 2015. **7**(45): p. 25180-25192.
30. Zeng, R., et al., *Corrosion of molybdate intercalated hydrotalcite coating on AZ31 Mg alloy*. Journal of Materials Chemistry A, 2014. **2**(32): p. 13049-13057.
31. Wang, Y. and D. Zhang, Synthesis, characterization, and controlled release anticorrosion behavior of benzoate intercalated Zn–Al layered double hydroxides. Materials Research Bulletin, 2011. **46**(11): p. 1963-1968.
32. Cao, Y., et al., Multifunctional inhibition based on layered double hydroxides to comprehensively control corrosion of carbon steel in concrete. Corrosion Science, 2017. **126**: p. 166-179.

33. Cao, Y., et al., A composite corrosion inhibitor of MgAl layered double hydroxides co-intercalated with hydroxide and organic anions for carbon steel in simulated carbonated concrete pore solutions. Journal of The Electrochemical Society, 2019. **166**(11): p. C3106-C3113.
34. Xu, T., et al., Composite nanocontainers synthesized by in-situ growth of metal organic frameworks on layered double hydroxides having both passive and active protecting capabilities. Progress in Organic Coatings, 2022. **164**: p. 106695.